

The electronic structure of the $\text{CuRh}_{1-x}\text{Mg}_x\text{O}_2$ thermoelectric materials: An X-ray photoelectron spectroscopy study

T.K. Le ^a, D. Flahaut ^{a,*}, H. Martinez ^a, N. Andreu ^a, D. Gonbeau ^a, E. Pachoud ^b, D. Pelloquin ^b, A. Maignan ^b

^a IPREM/ECP (UMR 5254), University of Pau, Hélioparc, 2 av. Pierre Angot, 64053 Pau Cedex 9, France

^b Laboratoire CRISMAT, UMR 6508 CNRS-ENSICAEN and IRMA FR3095, 6 Boulevard Maréchal Juin, Caen Cedex 4, France

ARTICLE INFO

Article history:

Received 26 February 2011

Received in revised form

30 June 2011

Accepted 6 July 2011

Available online 19 July 2011

Keywords:

XPS

Delafoseite

Rh3d

Thermoelectric properties

ABSTRACT

A detailed X-ray photoelectron spectroscopy study has been performed for the $\text{CuRh}_{1-x}\text{Mg}_x\text{O}_2$ ($x=0, 0.04$ and 0.10) series for a better understanding of the role of the Mg^{2+} substitution on the electrical properties and the value of the Seebeck coefficient. This study is based on an analysis of different compounds such as Rh_2O_3 , Sr_2RhO_4 and CuCrO_2 in order to characterize different oxidation states (Rh^{3+} and Rh^{4+} in octahedral oxygen environment and Cu^{+} in a dumbbell O–Cu–O coordination). The $\text{Cu}2p$ signal of copper in the non-doped compounds CuCrO_2 and CuRhO_2 reveals different electronic structures. An evolution of the $\text{Cu}2p$ core signal with the increase of Mg^{2+} content in the $\text{CuRh}_{1-x}\text{Mg}_x\text{O}_2$ is highlighted by XPS. The differences observed, especially for the $\text{Cu}2p$ core peaks are discussed for the non-doped compounds CuCrO_2 and CuRhO_2 as for the $\text{CuRh}_{1-x}\text{Mg}_x\text{O}_2$ series upon Mg^{2+} substitution.

© 2011 Elsevier Inc. All rights reserved.

1. Introduction

Cobalt-based layer oxides with CdI_2 -type CoO_2 layers, such as Na_xCoO_2 or misfit layered compounds, in which the cobalt cations adopt a low-spin (LS) state, show interesting thermoelectric properties with the best ZT values ($ZT=S^2T/\rho\kappa$, where S , T , ρ and κ represent the thermopower, absolute temperature, electrical resistivity and thermal conductivity, respectively) at high temperature among oxides. In that respect, the CuMO_2 delafossite structures are very interesting in particularly those, which revealed a high figure of merit ZT : 0.14 at 1100 K for $\text{CuFe}_{0.99}\text{Ni}_{0.01}\text{O}_2$ [1], 0.04 at 800 K for $\text{CuCr}_{0.97}\text{Mg}_{0.03}\text{O}_2$ [2] and 0.15 at 1000 K for $\text{CuRh}_{0.90}\text{Mg}_{0.10}\text{O}_2$ [3]. The delafossite structure possesses MO_6 sheets isostructural to the CoO_6 layer of Na_xCoO_2 . It differs by the interlayer connection as the MO_2 sheets in CuMO_2 delafossite are joined by Cu cations, which form bridges between O ions in the adjacent sheets, yielding a 3D structure. The lower electrical resistivities were reported for CuCrO_2 and CuFeO_2 , for which it is believed that the favourable mixing of the Cu–O orbitals with the $3d$ states of the M^{III} cation in the Cu–O–MIII–O–Cu linkages is providing a pathway for holes. As illustrated by DOS calculation carried out on CuCrO_2 , the chromium states generate an oxygen mediated effect on the Cu d states at the top of the valence band [4].

Part of the problem concerning the holes transfer in delafossites might be related to their oxygen non-stoichiometry. When the M cation exceeds a certain size, the incorporation of extra oxygen

anions is favoured in the copper layer [5]. This is the case for CuLaO_{2+x} , CuYO_{2+x} and CuFeO_{2+x} [6]. This oxygen intercalation of oxide ions can create an oxidation of Cu^{+} to Cu^{2+} into the $\text{Cu}^{+}\text{M}^{3+}\text{O}_2$ delafossites and might influence the physical properties. In this way, Scanlon et al. [7] have widely discussed the electrical resistivity evolution of Cu^{+}MO_2 ($\text{M}^{3+}=\text{Al, Cr, Sc and Y}$) compounds versus the cationic M^{3+} size. An increase in the size of M^{3+} cation and consequently oxygen intercalation is responsible for the larger electrical conductivity of CuYO_2 than CuScO_2 whereas CuCrO_2 exhibits the largest electrical conductivity. Indeed the in-plane Cu–Cu distance cannot be the only factor determining the electrical conductivity and the impact of the interactions between Cr and O ions on the electronic density on the top of the valence band has to be considered [4].

Among the delafossite structures, Mg-doped CuCrO_2 exhibits also interesting thermoelectric properties for which the origin is still under debate [8]: the Cu or CrO_2 or both layers may be engaged in the electrical transport [9]. Recently, the Mg-doped CuRhO_2 series has been investigated by electronic calculations and transport measurements [10]. It has been reported to be a promising candidate for thermoelectricity (Power Factor=0.7 mW K $^{-2}$ m $^{-1}$ at $T=900$ K). Due to the larger ionic radius of the Rh^{3+} cation ($r_{\text{Rh}}^{3+}=0.665$ Å) than Cr^{3+} ($r_{\text{Cr}}^{3+}=0.615$ Å), 12% of Mg^{2+} can be substituted for Rh in CuRhO_2 , instead of 1% for Cr in CuCrO_2 [8]. The conduction path in the CuRhO_2 delafossite is controversial: conduction through both the Cu and RhO_2 layers [9] or an electrical conduction governed only by the RhO_2 layer [10]. Based on electronic band calculations, it was proposed that the transport is dominated by the $\text{Rh}4d$ bands. However, the role of the Cu channel to the electronic transport has to be considered in relation with the insulator–metal transition [10].

* Corresponding author. Fax: +33 5 59 40 76 22.

E-mail address: delphine.flahaut@univ-pau.fr (D. Flahaut).

which is unusual for a CuMO₂ delafossite. In addition, contrasting to CuCrO₂, the CuRhO₂ compound could exhibit an oxygen non-stoichiometry due to the larger ionic radius of the Rh³⁺ cation.

The aim of this work is to contribute to a better understanding of the Mg substitution role on the electrical properties and the Seebeck coefficient by considering the electronic evolutions in the delafossite series. In this way, we report on a XPS study of CuCrO₂/CuRhO₂ compounds and of the CuRh_{1-x}Mg_xO₂ series. The XPS study is undertaken on the basis of combined analysis of core peaks and valence bands. The analysis of core peaks associated with their chemical shift provides the characterization of local chemical environment of atoms and also of oxidation numbers. The valence band spectra, related to the occupied density of states, correspond to a secondary probe and provide complementary information. This investigation has been based on fine studies of the core peaks of reference samples.

2. Experiment

Polycrystalline samples of CuRh_{1-x}Mg_xO₂ ($x=0, 0.04$ and 0.1) were prepared via solid state reactions in air. The precursors Cu₂O, Rh₂O₃ and MgO were mixed in the stoichiometric ratio. The products were pressed in the form of bars under 1 ton/cm² and calcined at 1050 °C for 12 h. The CuCrO₂ sample has been

Table 1
XPS data of Sr₂RhO₄ and Rh₂O₃ compounds: binding energies (eV), FWHM (eV) in parentheses and atomic percentages (%).

Core peaks	Sr ₂ RhO ₄			Rh ₂ O ₃		
	B.E.	FWHM	%	B.E.	FWHM	%
Sr 3d_{5/2}	131.7	1.0	1.2			
	133.6	1.7	6.1			
Rh 3d_{5/2}	309.3	1.6	2.0	308.8	0.7	18.4
				311.6	1.0	1.2
				312.8	1.0	1.4
O1s	529.0	2.0	2.8	530.4	0.9	37.3
	531.6	1.7	20.3	531.7	1.6	9.5
	533.4	2.5	7.9	533.5	1.5	3.5
C1s	285.0	1.2	28.9	285.0	0.9	23.5
	286.4	2.0	21.3	286.4	1.6	2.2
	289.4	2.0	9.5	288.4	1.5	2.8

Table 2
XPS data of CuCrO₂ and CuRh_{1-x}Mg_xO₂ delafossite: binding energies (eV), FWHM (eV) in parentheses and atomic percentages.

Core peaks	CuCrO ₂			CuRhO ₂			CuRh _{0.96} Mg _{0.04} O ₂			CuRh _{0.90} Mg _{0.10} O ₂		
	B.E.	FWHM	%	B.E.	FWHM	%	B.E.	FWHM	%	B.E.	FWHM	%
Cu 2p_{3/2}	932.3	1.2	11.1	932.4	1.1	10.1	932.4	1.3	7.2	932.4	1.2	11.2
				934.8	2.1	2.3	934.8	2.0	2.5	934.6	2.3	4.6
	936.9	1.3	0.3	936.9	1.3	0.3	936.9	1.3	0.2	936.9	1.3	0.4
				941.3	2.6	1.1	941.2	2.6	0.9	941.6	2.6	1.8
				944.0	2.6	1.1	943.9	2.6	0.9	944.3	2.6	1.8
Cr 2p_{3/2}	943.8	2.4	0.3	943.7	2.0	0.3	943.4	1.9	0.2	943.8	2.5	0.3
	946.6	1.3	0.3	946.6	1.1	0.3	946.6	1.3	0.2	946.6	1.3	0.3
Cr 2p_{1/2}	576.3	3.0	12.4									
Rh 3d_{5/2}				308.6	0.7	12.0	308.6	0.7	10.6	308.6	0.8	10.2
				311.8	0.9	0.9	311.8	1.1	1.1	311.9	0.9	0.8
				312.6	0.9	1.3	312.7	0.9	1.2	312.7	0.9	1.1
O1s	530.0	1.2	36.8	530.2	0.9	30.6	530.1	1.0	27.4	530.1	1.2	33.1
	531.8	2.1	17.9	531.4	1.6	15.2	531.5	1.9	19.6	531.5	1.7	16.7
C1s	285.0	1.6	17.4	285	1.2	19.9	285	1.2	22.0	285	1.2	15.2
	286.8	1.1	1.7	286.4	1.2	1.6	286.3	1.3	3.5	286.3	1.5	3.3
	288.6	1.7	1.9	288.9	1.2	1.7	288.8	2	2.8			

prepared also by solid state reaction by mixing Cu₂O and Cr₂O₃ in the stoichiometric ratio. The powders were pressed into bars and calcined at 1200 °C for 12 h in air. The Sr₂RhO₄ compound was prepared by mixing SrO and Rh₂O₃ in the stoichiometric ratio. The powder was heated at 1200 °C during 12 h and then at 1250 °C during 35 h under oxygen flow.

The low temperature ($T < 320$ K) electrical resistivity (ρ) and the Seebeck coefficient (S) were measured using a Quantum Design cryostat. The four-probe and the steady-state techniques were used, for both measurements, indium electrical contacts having been deposited with ultrasons. For the high temperature ρ and S measurements ($T > 300$ K) a Ulvac-Zem 3 system was used.

XPS analyses were carried out with a Kratos Axis Ultra spectrometer using a focused monochromatized Al $K\alpha$ radiation ($h\nu = 1486.6$ eV). The analyzed area of the samples was $300 \mu\text{m} \times 700 \mu\text{m}$, and the pressure in the analysis chamber was ca. 5×10^{-9} Pa. The samples, which are in form of bars, are cleaved and installed on the sample holder directly in the glove box (1 ppm in O₂ and H₂O) connected to the spectrometer, to avoid oxidation and contamination of the surface by reaction with the ambient atmosphere. The binding energy scale was calibrated from the carbon contamination (always present at surface of materials) using the C1s peak at 285 eV. Core peaks were analyzed using a nonlinear Shirley-type background, and peak positions and areas were obtained by a weighted least-square fitting of model curves (70% Gaussian, 30% Lorentzian) to the experimental data. Quantification was performed on the basis of Scofield's relative sensitivity factors [11].

3. Results

The XPS investigations of CuRh_{1-x}Mg_xO₂ samples requires further studies of reference phases having a well defined structure to characterize the formal oxidation number: Cu²⁺ (CuO), Cu⁺ (Cu₂O), Rh³⁺ (Rh₂O₃) and Rh⁴⁺ (Sr₂RhO₄). Cu2p, Cr2p, Rh3d, O1s, C1s and Sr3d core peaks have been recorded. The data of the most relevant compounds are reported in Tables 1 and 2.

3.1. References materials

3.1.1. Copper oxides

Several XPS studies have been carried out on copper oxides and the different signatures of CuO and Cu₂O are well known. The

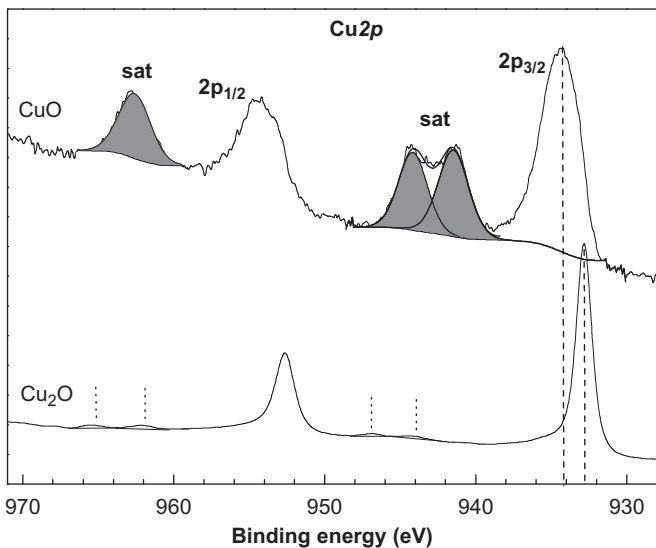


Fig. 1. Cu2p spectra of CuO and Cu2O. Low intensity peaks are marked with vertical bars in Cu2O and satellites of the Cu2p components with filled peaks in CuO.

Cu2p peaks of CuO and Cu2O are shown in Fig. 1. The spectrum of the CuO oxide is representative of the divalent copper Cu²⁺ (3d⁹4s⁰) in an oxygen environment. The main Cu2p components of CuO are relatively broad and are located at 934.4 eV (Cu2p_{3/2}) and 954.2 eV (Cu2p_{1/2}). Each peak presents an intense satellite at 8 eV above the 2p_{3/2} and 2p_{1/2} peaks positions. The $I_{\text{sat}}/I_{\text{main}}$ peak ratio value is 0.62. This “shake-up” satellite results from metal-ligand charge transfer during the photoemission process, characteristic of copper oxides having a d⁹ configuration in the ground state [12,13]. The Cu2p spectra of Cu2O sample (Fig. 1) is representative of monovalent copper with two oxygen in a linear O–Cu–O arrangement. The Cu⁺ can be identified by a well defined Cu2p_{3/2-1/2} doublet (Binding Energy (BE) at 932.3 and 952.2 eV). Small peaks of low intensity appear on the high binding energy side of the Cu2p main components, in particular at 11 and 14 eV. These peaks have been assigned to the presence of excited final state satellites associated with minor contributions from Cu d⁹ initial state configurations [14]. These results evidence clear differences between the Cu2p core peaks of Cu2O and CuO.

3.1.2. Rhodium oxides

The Rh3d spectra of the reference compounds are shown in Fig. 2. The Rh₂O₃ corundum structure is representative of trivalent Rh (4d⁶5s⁰) and the K₂NiF₄-type phase Sr₂RhO₄ of tetravalent Rh (4d⁵5s⁰) in a RhO₆ edge-shared octahedron. The Sr₂RhO₄ compound crystallizes in a tetragonal structure with a reduced I₄₁/acd symmetry due to a 11° rotation of the RhO₆ octahedra around the c-axis [15].

For the Rh₂O₃ sample, Fig. 2 shows, in agreement with previous work [16], a well-resolved Rh3d_{5/2} component centred at 308.8 eV (Full Width at Half Maximum (FWHM) ~0.7 eV) and a Rh3d_{3/2} component at 313.7 eV assigned to Rh³⁺ species. Satellite peaks located at 3.2 and 4 eV above the Rh3d_{5/2} peak are also observed. Note that the satellites associated to Rh3d_{3/2} component are hardly discernable due to the low $I_{\text{sat}}/I_{\text{main}}$ peak ratio. The main component of O1s core peak is associated to BE of 530.4 eV.

To establish the signature of a Rh⁴⁺ in an oxide compound, Sr₂RhO₄ has been synthesized and characterized by XPS for the first time. This compound contains Rh⁴⁺ cation (4d⁵5s⁰) associated to BE of 309.3 eV (FWHM ~1.6 eV) (Fig. 2). It has to be noted that no satellite and an asymmetry on the left side of the

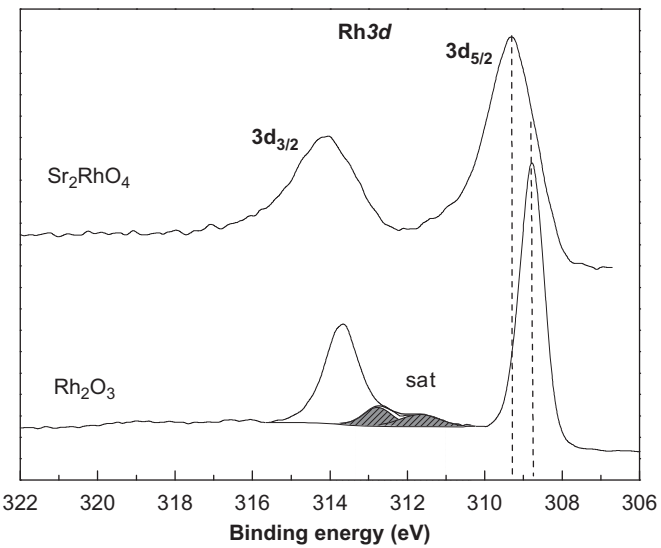


Fig. 2. Rh3d spectra of Rh₂O₃ and Sr₂RhO₄ samples. The filled peaks are assigned to the satellites of the Rh3d_{5/2} component.

peak are observed. In addition, the O1s core peak is centered at 529 eV. The $\Delta_{\text{BE}}(\text{O1s}-\text{Rh3d})$ values have also been determined: 221.6 eV for Rh₂O₃ compared to 219.7 eV for Sr₂RhO₄. These differences inform on the electronic redistribution along Rh–O bonds and have the practical advantage to be independent of any calibration process. Thus, the difference of chemical environment for the oxygen ions in Sr₂RhO₄ (oxygen shared with Rh⁴⁺ and Sr²⁺) and Rh₂O₃ have to be considered. Previous work on alkaline-earth oxides [17] reported that the BE of O1s core peak in SrO material is around 527.7 eV while it is of 530.4 eV in Rh₂O₃. Consequently, the shift of the O1s peak of Sr₂RhO₄ towards lower binding energies is probably mainly due to their Sr cation neighbours.

The shift towards higher energies, that we observed, for Rh⁴⁺ (Sr₂RhO₄) as compared to Rh³⁺ (Rh₂O₃) is consistent with recent results obtained for Rh₂O₃ and RhO₂ compounds on the Spring 8-BL17U beam line [18].

3.2. Delafossite compounds

3.2.1. Structural characterization and physical properties

The CuRh_{1-x}Mg_xO₂ ($x=0$, 0.04 and 0.1) and CuCrO₂ samples crystallize in the delafossite structure ($R\bar{3}m$ space group). The (Rh/Mg) and Cr cations are located in distorted edge-shared (Rh/Mg)O₆ or CrO₆ octahedra (CdI₂-type) linked through a Cu cation linearly coordinated with two oxygen anions. Despite the fact that octahedra are slightly compressed along the threefold axis, the six (Cr/Rh)–O distances are equivalent.

All the polycrystalline samples CuRh_{1-x}Mg_xO₂ and CuCrO₂ were characterized by XRPD and EDS coupled to electron diffraction in previous works [8,10]. For CuRh_{1-x}Mg_xO₂, a small decrease of both a and c lattice parameters is observed when x_{nominal} increases up to 15%, which characterize the Mg substitution at the octahedral site. The Mg²⁺ maximum solubility is limited to 12%, and for larger substitution the Cu₂MgO₃ oxide is detected as a secondary phase. In the delafossite structure, the MO₂ layers are very compact, which could explain the very low substitution rate. For that reason, all the measurements and XPS experiments have been limited to $x \leq 0.10$.

The substitution of Rh cations in CuRhO₂ by Mg²⁺ cation induces a drastic decrease of the electrical resistivity values by a factor of 300 at $T=300$ K as x increases from 0.00 to 0.10 [10]. The CuRh_{1-x}Mg_xO₂

series with $x=0$ and 0.04 exhibits a localized behaviour in contrast with the electrical resistivity curve of $\text{CuRh}_{0.9}\text{Mg}_{0.1}\text{O}_2$, which shows a metallic behaviour over all the T range from $5 \times 10^{-3} \Omega \text{ cm}$ at 800 K down to $1.2 \times 10^{-3} \Omega \text{ cm}$ at 5 K. This insulating to metal transition lets us consider the exact role of the Cu channel in the electrical properties as well as in the Seebeck (S) coefficient evolution. The decrease of the S value as x increases in $\text{CuRh}_{1-x}\text{Mg}_x\text{O}_2$ together with the positive value of S (p-type charge carriers) is consistent with an increase of the hole fraction induced by the charge compensation created by the Mg^{2+} for Rh^{3+} substitution. The highest power factor is obtained for the $\text{CuRh}_{0.9}\text{Mg}_{0.1}\text{O}_2$ compound at 1000 K with the value of $7 \times 10^{-4} \text{ W K}^{-2} \text{ m}^{-1}$ close to that reported for p-type layer cobaltites as the misfit ones [19]. The S evolution and the transport properties were interpreted by Maignan et al. [10] as a creation of Rh^{4+} holes according to the formula $\text{CuRh}_{1-2x}\text{Rh}_x^{4+}\text{Mg}_x^{2+}\text{O}_2$.

3.2.2. CuRhO_2 and CuCrO_2

As previously reported, both non-substituted compounds CuRhO_2 and CuCrO_2 are insulating with very different Seebeck values (280 and $1100 \mu\text{V K}^{-1}$, respectively) and a larger electrical conductivity for the CuRhO_2 compound; it is to be noted that the origin of those different electrical properties is still not clear.

First of all, we investigate by XPS those non-doped compounds and more particularly the signature of the $\text{Cu}2p$ and $\text{Rh}3d$ core peaks. The $\text{Cu}2p$ spectra of CuCrO_2 sample (Fig. 3), similar to the one obtained for Cu_2O , (Fig. 1) is representative of monovalent copper in a two-fold oxygen environment. The Cu^+ is well identified by a $\text{Cu}2p_{3/2-1/2}$ doublet (BE at 932.3 eV (A) and 952.2 eV (A')). Small peaks (A_{sat} and A'_{sat}) of low intensity are observed at 5, 11 and 14 eV above the A and A' peak positions. The binding energy of the $\text{Cr}2p_{3/2}$ peak (576.3 eV) (not shown here) is characteristic of a trivalent oxidation state for the chromium cation [20,21].

Fig. 4 ($x=0$) exhibits the $\text{Cu}2p$ spectrum of CuRhO_2 . We focus on the well defined lower BE part of this spectrum. The main $\text{Cu}2p_{3/2}$ components are located at 932.4 eV (A) and 934.8 eV (B), with lower intensity peaks located at higher binding energy. Based on the reference materials (Cu_2O and CuO), the A and B peaks are, respectively, associated with the Cu^+ and Cu^{2+} oxidation states, which implies a Cu^{+2+} mixed-valency for the copper cations in CuRhO_2 . The shift to higher BE (+0.4 eV) of the $\text{Cu}2p_{3/2}$ main component (B) (relative to Cu^{2+}) as compared to the CuO reference compound can be attributed to some change in the electronic distribution around copper induced by different chemical and

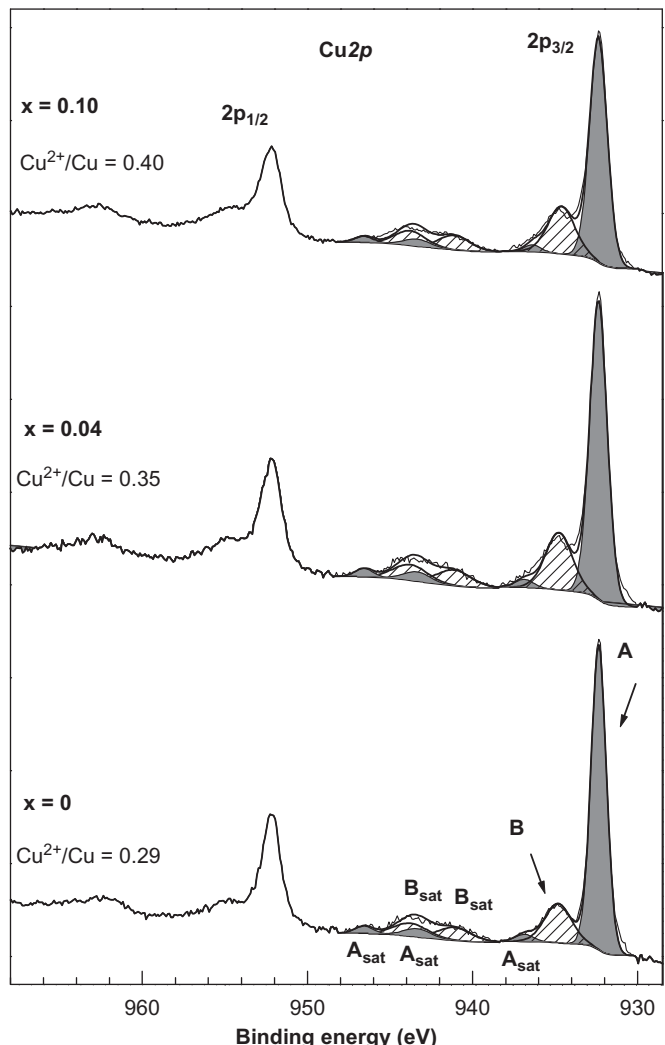


Fig. 4. $\text{Cu}2p$ spectra of the $\text{CuRh}_{1-x}\text{Mg}_x\text{O}_2$ series as a function of x ($x=0, 0.04$ and 0.1). The filled peaks are assigned to main peak A and A_{sat} satellites, the hatched peaks to main peak B and B_{sat} satellites.

structural environments in those two materials. The copper cation is linked to two oxygen anions in the oxygen stoichiometric delafossite instead of four in the CuO cupric oxide. It is to remember the formal character of oxidation numbers that correspond to entire charges whereas, in reality, many gradations exist.

Taking into account the results obtained for the reference compounds, the $\text{Cu}2p_{3/2}$ spectrum of CuRhO_2 has been fitted by considering the characteristic (main peak and satellites) of the Cu^+ and Cu^{2+} signatures. The three low intensity peaks, located at 936.9, 943.7 and 946.6 eV (A_{sat}), have been assigned to the Cu^+ and the two satellites (B_{sat}) at 941.3 and 944 eV to the Cu^{2+} oxidation states. As the Cu signal is related to a mixed valency Cu^{+2+} , the Cu^{2+}/Cu ratio can be calculated. The relative concentration of the Cu^{2+} species can be obtained as follows $\text{Cu}^{2+}/\text{Cu} = (B + B_{\text{sat}})/(A + A_{\text{sat}} + B + B_{\text{sat}})$, where B is the contribution of the Cu^{2+} main peak, B_{sat} is one of the shake-up peaks of the Cu^{2+} component, A the contribution of the Cu^+ main peak and A_{sat} is the corresponding satellites [22]. In CuRhO_2 , the calculated value is equal to 0.29. Considering the drastic analysis conditions (the samples are cleaved before each analysis in a glove box directly connected to the XPS analysis chamber), a surface oxidation of our samples is excluded.

The $\text{Rh}3d$ spectrum (Fig. 5, $x=0$) corresponds to two components $\text{Rh}3d_{5/2}$ and $\text{Rh}3d_{3/2}$ located at 308.6 and 313.6 eV, respectively, and

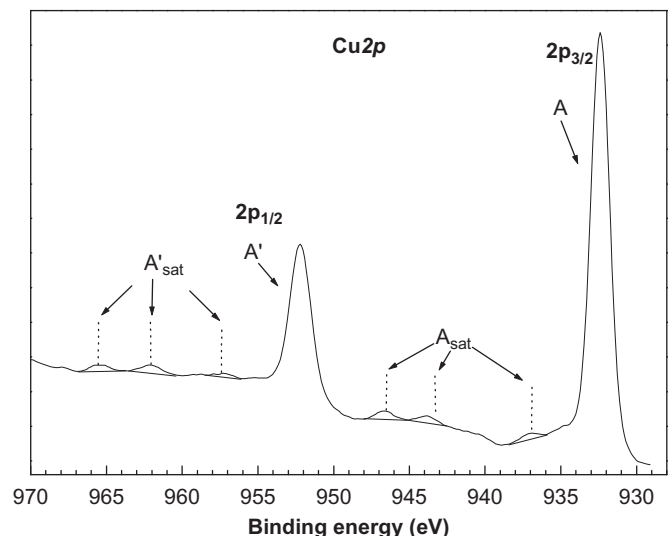


Fig. 3. $\text{Cu}2p$ spectrum of CuCrO_2 . The vertical bars point the small peaks (A_{sat} and A'_{sat}) at 5, 11 and 14 eV from the main components (A and A').

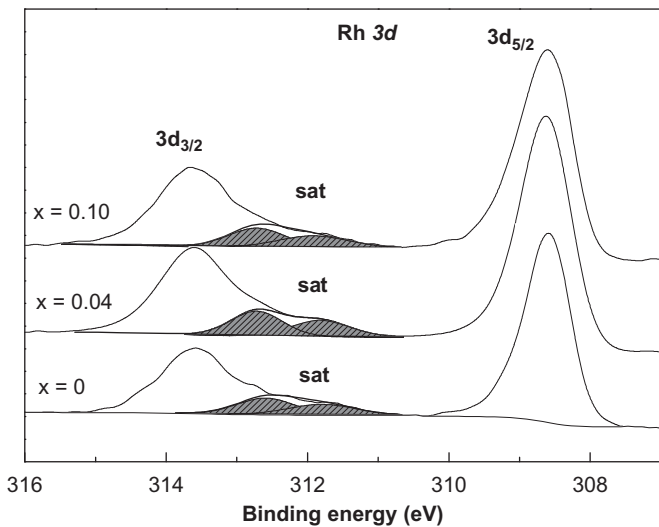


Fig. 5. Rh3d spectra of the CuRh_{1-x}Mg_xO₂ series as a function of x ($x=0, 0.04$ and 0.10). The filled peaks are assigned to the satellites of the Rh3d_{5/2} component.

satellite peaks associated to the Rh3d_{5/2} component. The BE and the FWHM values are similar to those reported for Rh₂O₃ despite a difference in the $\Delta_{\text{BE}}(\text{Rh3d}_{5/2}-\text{sat})$ values between Rh₂O₃ and CuRhO₂. As this Δ_{BE} between the main peak and satellite depends on the total chemical environment of the considered atom, it might be related in this case to the difference in the second neighbors of the rhodium in those materials (6 Rh³⁺ and 4 Rh³⁺, respectively, for the CuRhO₂ and Rh₂O₃ compounds).

3.2.3. CuRh_{1-x}Mg_xO₂

For the CuRh_{1-x}Mg_xO₂ series, we have to note that the XPS analyses of these compounds confirm the insertion of Mg in CuRhO₂ delafossite as the Mg Auger peak has been detected at 304 eV for $x=0.04$ and 0.10 .

The Cu2p and Rh3d core peaks of the CuRh_{1-x}Mg_xO₂ compounds are shown in Figs. 4 and 5. First, the Mg substitution do not affect the Rh3d core peaks in the CuRh_{1-x}Mg_xO₂ series ($x=0-0.04-0.10$). Neither the global shapes of the spectra nor the binding energies vary whatever the composition is. Moreover, the ionic character of the O–Rh bond ($\Delta_{\text{BE}}(\text{O}1s-\text{Rh}3d)=221.5$ eV) remains unchanged by the magnesium substitution, which confirms predominance of the Rh³⁺ oxidation state. However on the basis of these data, it is not possible to exclude a small amount of Rh⁴⁺ oxidation state.

The analyses of the Cu2p_{3/2} peaks (BE and FWHM) have been realized carefully taking into account the characteristics deduced from the analysis of CuRhO₂. In particular, we kept the intensity ratio ($I_{\text{Bsat}}/I_{\text{B}} \sim 0.8$) along the series. An increase of the component relative to the Cu²⁺ signature is observed in the Cu2p spectra (Fig. 4). The Cu²⁺/Cu ratio, calculated as describing previously, increases with x , from 0.29 for $x=0$, to 0.35 for $x=0.04$ and to 0.40 for $x=0.10$. All the Cu2p spectra of the CuRh_{1-x}Mg_xO₂ exhibit the same behaviour. The binding energies and the $\Delta_{\text{BE}}(\text{Cu2p}_{3/2}(A)-\text{Cu2p}_{3/2}(B))$ values are unchanged for all the Mg content ($x=0$ to 0.10).

Therefore, the main result here obtained is that the Mg substitution at the Rh sites in the CuRh_{1-x}Mg_xO₂ ($x=0.04-0.1$) samples produces a hole creation (increasing with x) at the Cu site by charge compensation.

3.3. Valence spectra

The valence bands of the series CuRh_{1-x}Mg_xO₂ ($x=0, 0.04$ and 0.10) are displayed in Fig. 6. The spectrum of CuRhO₂ can be

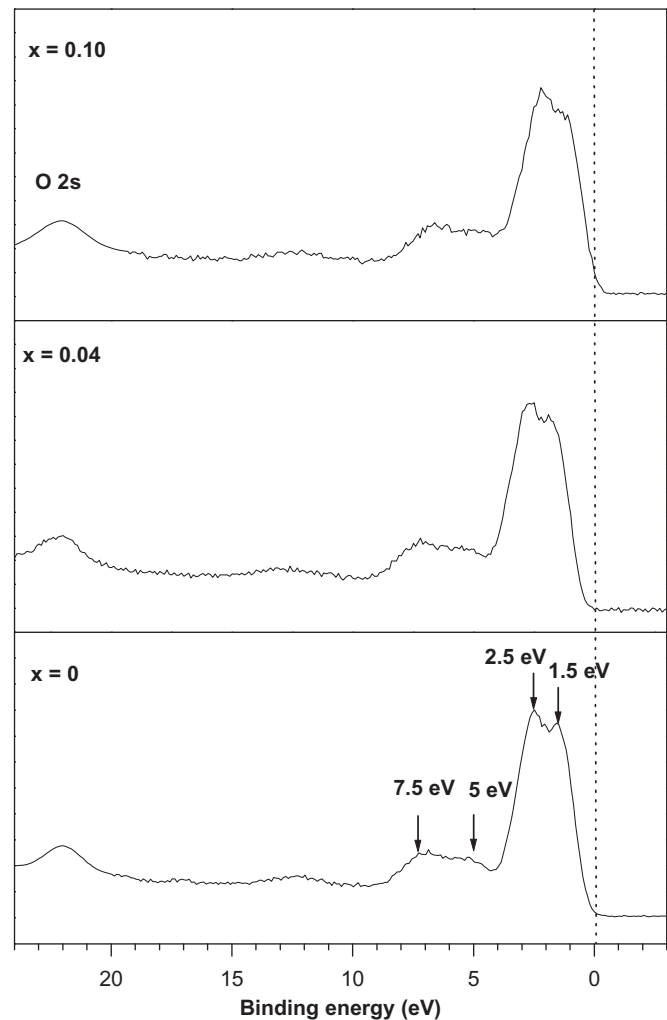


Fig. 6. Valence spectra of the CuRh_{1-x}Mg_xO₂ series as a function of x ($x=0, 0.04$ and 0.10).

interpreted on the basis of previous calculations [10], pointing out that the transport is dominated by the Rh4d band. Indeed the main peaks at 1.5 and 2.5 eV are mainly attributed, respectively, to the Rh4d (t_{2g}) and Cu3d states. The cross section ratio $\sigma(\text{Rh}4d)/\sigma(\text{Cu}3d)$ is equal to 1:0.65 but the nominal electron count is greater for Cu. Moreover, a fine analysis of the results shows that these states near the Fermi level also correspond to some Cu3d–Rh4d hybridized states [10]. The peaks at 5 and 7.5 eV mainly result from interactions between O2p and Rh4d orbitals. Indeed, the σ -type overlap of the O2p states with the Rh4d e_g orbitals leads to the contribution of the latter between 5 and 7 eV. For the substituted samples, the valence bands are very similar. Nonetheless, we can observe a subtle variation of the intensity ratio between $I(\text{Cu}3d)$ and $I(\text{Rh}4d)$.

We also note a non-zero density of states at the Fermi level for CuRh_{0.9}Mg_{0.1}O₂, which is not observed for the $x=0$ and 0.04 compounds. Inspecting the transport measurements [10], the valence band evolution is consistent with the insulator–metal transition in the CuRh_{1-x}Mg_xO₂ series observed for $x=0.1$.

4. Discussion

As it has been previously reported, both non-substituted compounds CuRhO₂ and CuCrO₂ are insulating with very different Seebeck values 280 and 1100 $\mu\text{V K}^{-1}$, respectively. First of all, the

different values of electrical resistivity and the Seebeck coefficient measured for the CuRhO_2 and CuCrO_2 delafossite could be connected to the different $\text{Cu}2p$ core peak signatures. XPS analyses ($\text{Cu}2p$ spectra) give evidence for different oxidation states of copper between CuCrO_2 and CuRhO_2 . The CuCrO_2 compound does not exhibit any Cu^{2+} contribution whereas CuRhO_2 presents a Cu^{2+}/Cu ratio of 0.29. This is well correlated with the high Seebeck value reported for CuCrO_2 ($S_{300\text{ K}} \sim 1100 \mu\text{V K}^{-1}$; $1 \times 10^{-5} \text{ Cu}^{2+}$ per site Cu) and the lower one for CuRhO_2 ($S_{300\text{ K}} \sim 300 \mu\text{V K}^{-1}$), i.e. concentration of hole charge carriers expected much larger in the latter. The neutron powder diffraction study of CuCrO_2 [23] supports this hypothesis: its oxygen content “O₂” is stoichiometric implying the existence of trivalent chromium cations. Indeed our results show that copper in the CuCrO_2 delafossite is only monovalent. Concerning the undoped CuRhO_2 compound the existence of a $\text{Cu}^+/\text{Cu}^{2+}$ mixed valency may be due to significant quantity of extra oxygen anions intercalated into the $\text{Cu}^+\text{Rh}^{3+}\text{O}_2$. Thus the created Cu–O–Rh–O–Cu linkages could provide a pathway for holes [24] and explain the lower electrical resistivity of CuRhO_2 . Moreover the fact that the rate of oxygen insertion in the copper plane is not checked, might explain the different values of Seebeck coefficient reported in the literature for the CuRhO_2 delafossite [10,25].

The originality of the $\text{CuRh}_{1-x}\text{Mg}_x\text{O}_2$ physical properties lies in the fact that a sharp decrease of the electrical resistivity and the Seebeck coefficient is occurring for low Mg^{2+} substitution in the CdI_2 -type layer. It is to be noted that some author mentioned a hole creation by charge compensation [8]. Concerning these Mg-doped samples, a mixed valency $\text{CuRh}_{(1-2x)}\text{Rh}_x^{4+}\text{Mg}_x^{2+}\text{O}_2$ has been proposed [10] whereas, according to magnetoresistance experiments, others [8] proposed the possibility of a Cu^{+2+} mixed-valency. Our results from XPS measurements demonstrate that the main change induced by the Mg^{2+} substitution is the creation of Cu^{2+} identified by the analyses of the $\text{Cu}2p$ peak. It is important to note that the contribution of surface oxidation cannot be responsible for this creation of Cu^{2+} since drastic experimental conditions have been carried out to avoid any surface degradation. It is to be also noted that Zheng et al. [26] have also observed a Cu^{+2+} mixed valency for Ni doped CuCrO_2 delafossite ($\text{CuCr}_{0.94}\text{Ni}_{0.06}\text{O}_2$). Moreover, we have discussed carefully of the oxidation state of the rhodium cation in those samples as the binding energy difference between Rh^{4+} and Rh^{3+} is rather small. If in $\text{CuRh}_{1-x}\text{Mg}_x\text{O}_2$ the rhodium cations adopt a Rh^{3+4+} mixed-valency state, the latter seems not to be affected by the change of Mg content. Although most of the physical measurements tend to explain the transport mechanism by a Cr–O or Rh–O conducting network, our data do not clearly evidence such result. Moreover, the $\text{CuRh}_{0.9}\text{Mg}_{0.1}\text{O}_2$ develops metal-like transport which has not been observed in other delafossite. The insulator–metal like transition observed from transport measurements is well correlated with the valence band signature at the Fermi level for this compound.

For the $\text{CuRh}_{1-x}\text{Mg}_x\text{O}_2$ series, we conclude to the simultaneous increase of the Cu^{2+}/Cu ratio induced by charge compensation created by the Mg^{2+} for Rh^{3+} substitution and the presence of a non-zero density of states at the Fermi level for $x=0.1$.

As a strong hybridization of the Cu–O–Rh pathway associated to a strong covalency of the Cu–O–Rh bond have been reported from XPS and theoretical calculation studies, this gives further support to the hypothesis that a conduction path through the Cu–O–Rh–O channel is at work. So this study completes the work carried out by Maignan et al. [10] for which a transport dominated by the Rh4d bands was proposed. The approach based on photoemission spectroscopy analyses provides to better understand the complex conduction mechanism of those compounds.

5. Concluding remarks

XPS investigations have been carried out on reference compounds and the $\text{CuRh}_{1-x}\text{Mg}_x\text{O}_2$ ($x=0-0.04-0.1$) delafossites in order to better understand the influence of magnesium doping on to the electrical properties. We have shown a clear difference on the electronic state of the Cu cation for the two non-doped compounds CuCrO_2 and CuRhO_2 : the copper is in mixed-valency Cu^{+2+} for the undoped CuRhO_2 compound and in a monovalent state for CuCrO_2 . Moreover, we have evidenced that the copper cation keep two oxidation states $\text{Cu}^+/\text{Cu}^{2+}$ in the $\text{CuRh}_{1-x}\text{Mg}_x\text{O}_2$ ($x=0-0.4-0.1$) with an increase of the Cu^{2+}/Cu ratio with the x value. Therefore, the result shows that the Mg^{2+} substitution not only acts on the rhodium, but that the Cu^{2+}/Cu ratio evolves with the Mg^{2+} substitution. In addition, taking into account the previous results obtained by Maignan et al. [10], we propose a chemical formula for the $\text{CuRh}_{1-x}\text{Mg}_x\text{O}_2$ delafossite compounds, which could be written from a formal viewpoint as $\text{Cu}_{(1-2x)}\text{Cu}_x^{2+}\text{Rh}_{(1-2y)}^{3+}\text{Rh}_y^{4+}\text{Mg}_x^{2+}(x+y)\text{O}_2$. The contribution of the Cu layer can be reinforced by the metallic conductivity and the non-zero electronic density of states at the Fermi level observed for $\text{CuRh}_{0.9}\text{Mg}_{0.1}\text{O}_2$. This work points out the role of the copper cations in the complex electrical transport in such delafossites.

References

- [1] K. Hayashi, T. Nozaki, T. Kajitani, Jpn. J. Appl. Phys. 46 (2007) 5226; T. Nozaki, K. Hayashi, T. Kajitani, J. Chem. Eng. Jpn. 40 (2007) 1205.
- [2] Y. Ono, K. Satoh, T. Nozaki, T. Kajitani, Jpn. J. Appl. Phys. 46 (Part 1) (2007) 1071.
- [3] H. Kuriyama, M. Nohara, T. Sasagawa, K. Takubo, T. Mizokawa, K. Kimura, H. Takagi, Proceedings of 25th International Conference on Thermoelectrics IEEE, Piscataway, 97, 2006.
- [4] D.O. Scanlon, A. Walsh, B.J. Morgan, G.W. Watson, D.J. Payne, R.G. Eggle, Phys. Rev. B 79 (2009) 035101.
- [5] R.J. Cava, W.F. Peck, J.J. Krajewski, S.-W. Cheong, H.Y. Hwang, J. Mater. Res. 9 (1994) 314.
- [6] R.J. Cava, H.W. Zandbergen, A.P. Ramirez, H. Takagi, C.T. Chen, J.J. Krajewski, W.F. Peck Jr., J.V. Waszczak, G. Meigs, R.S. Roth, L.F. Schneemeyer, J. Solid State Chem. 104 (1993) 437.
- [7] D.O. Scanlon, K.G. Godinho, B.J. Morgan, G.W. Watson, J. Chem. Phys. 132 (2010) 024707.
- [8] A. Maignan, C. Martin, R. Frésard, V. Eyert, E. Guilmeau, S. Hébert, M. Poienar, D. Pelloquin, Solid State Commun. 149 (2009) 962.
- [9] S. Shibasaki, W. Kobayashi, I. Terasaki, Phys. Rev. B 74 (2006) 235110.
- [10] A. Maignan, V. Eyert, C. Martin, S. Kremer, R. Frésard, D. Pelloquin, Phys. Rev. B 80 (2009) 115103.
- [11] J.H. Scofield, J. Electron Spectrosc. Relat. Phenom. 8 (1976) 129.
- [12] J. Ghijssen, L.H. Tjeng, J. van Elp, H. Eskes, J. Westerink, G.A. Sawatzky, M.T. Czyzyk, Phys. Rev. B 38 (1988) 11322.
- [13] S. Hüfner, Solid State Chem. 17 (1975) 417.
- [14] S.L. Harmer, W.M. Skinner, A.N. Buckley, L.-J. Fan, Surf. Sci. 603 (2009) 537.
- [15] T. Vogt, D.J. Buttrey, J. Solid State Chem. 123 (1996) 186.
- [16] V.I. Nefedov, M.N. Firsov, I.S. Shaplygin, J. Electron Spectrosc. Rel. Phenom. 26 (1982) 65.
- [17] J.-C. Dupin, D. Gonbeau, P. Vinatier, A. Levasseur, Phys. Chem. Chem. Phys. 2 (2000) 1319.
- [18] A. Yamamoto, RIKEN Takagi Magnetic Materials Lab., private communication.
- [19] S. Okada, I. Terasaki, Jpn. J. Appl. Phys. 44 (2005) 1834.
- [20] J. Malherbe, H. Martínez, B. Fernández, C. Péchéyran, O.F.X. Donard, Spectrochim. Acta Part B 64 (2009) 155.
- [21] M.C. Biesinger, C. Brown, J.R. Mycroft, R.D. Davidson, N.S. McIntyre, Surf. Interface Anal. 36 (2004) 1550.
- [22] M.C. Biesinger, L.W.M. Lau, A.R. Gerson, R. StC Smart, Appl. Surf. Sci. 257 (2010) 887.
- [23] M. Poienar, F. Damay, C. Martin, V. Hardy, A. Maignan, G. André, Phys. Rev. 79 (2009) 014412.
- [24] J. Li, A.F.T. Yokochi, A.W. Sleight, Solid State Sci. 6 (2004) 831.
- [25] H. Kuriyama, M. Nohara, T. Sasagawa, K. Takubo, T. Mizokawa, K. Kimura, H. Takagi, in: Proceedings of 25th International Conference on Thermoelectrics, IEEE, Piscataway, 2006 p. 97.
- [26] S.Y. Zheng, G.S. Jiang, J.R. Su, C.F. Zhu, Mater. Lett. 60 (2006) 3871.